



HAL
open science

Two-scale finite element simulations for UT inspection of micro-structured materials in CIVA

Edouard Demaldent, Nicolas Leymarie, Vincent Dorval, Alexandre Imperiale,
Thibaud Fortuna

► To cite this version:

Edouard Demaldent, Nicolas Leymarie, Vincent Dorval, Alexandre Imperiale, Thibaud Fortuna. Two-scale finite element simulations for UT inspection of micro-structured materials in CIVA. WCNDT 2024, May 2024, Incheon, South Korea. pp.10.58286/29944, 10.58286/29944 . cea-04895339

HAL Id: cea-04895339

<https://cea.hal.science/cea-04895339v1>

Submitted on 17 Jan 2025

HAL is a multi-disciplinary open access archive for the deposit and dissemination of scientific research documents, whether they are published or not. The documents may come from teaching and research institutions in France or abroad, or from public or private research centers.

L'archive ouverte pluridisciplinaire **HAL**, est destinée au dépôt et à la diffusion de documents scientifiques de niveau recherche, publiés ou non, émanant des établissements d'enseignement et de recherche français ou étrangers, des laboratoires publics ou privés.



Two-scale finite element simulations for UT inspection of micro-structured materials in CIVA

Edouard Demaldent^{1*}, Nicolas Leymarie¹, Vincent Dorval¹, Alexandre Imperiale¹,
Thibaud Fortuna¹

¹ Université Paris-Saclay, CEA, List, F-91120, Palaiseau, France_

*Contact: edouard.demaldent@cea.fr

Abstract

Ultrasonic testing (UT) of highly heterogeneous structures is an important issue for many industrial applications in civil engineering for concrete inspection as well as in nuclear and oil & gas, where it applies to cast steels and weld joints. In these materials, performance is limited by the phenomenon of multiple wave scattering at the microstructure scale. In this context, the use of effective simulation tools is particularly useful both for improving interpretation of UT and for optimizing or demonstrating the performance of inspections. However, the scales of heterogeneity to be taken into account are often smaller than fractions of a tenth of a wavelength. In 3D simulations, it is therefore difficult, if not impossible, to combine computational performances with the refinement of the modelled interactions. To meet this challenge, CEA is developing an original approach based on two applications of the finite element (FE) method implemented in CIVA. The first application uses micro-scale heterogeneous material data on small representative elemental volumes (REVs) to feed a second code dedicated to macro-scale with effective medium characteristic. This second code relies on a high-order finite element model that is very efficient at the scale of the inspected industrial component. In this communication we present the main features of these FE tools and illustrate their performances on different application cases for welded parts and concrete

Keywords: Ultrasonic testing, Modelling, Finite Elements, Micro-structure, Weld Inspection

1. Motivations

Ultrasonic testing (UT) of highly heterogeneous structures is an important issue for many industrial applications in civil engineering as well as in nuclear and oil & gas, where it applies to cast steels and weld joints. Hereafter, the macroscopic scale (macro-scale) refers to the UT scale including the emission of a waveform, its propagation in the part and the phenomena of reflection and diffraction by an obstacle such as a defect. L_a designates the characteristic size of the macro-scale, of the order of the wavelength or of the width of the wave beam, which generally propagates over several tens of wavelengths in the part. A medium that is micro-structured with respect to the wavelength, i.e. whose elastic properties are heterogeneous at any point beyond a characteristic size $L_i \ll L_a$, influences the propagation speed and leads to attenuation of the wave beam, as well as structural noise on the received signal. A compact arrangement of grains is a typical example of a microstructure with regard to the inspection of a metal part. The texture of this microstructure, for example the direction of grain elongation in the chamfer of a weld, can also influence the directivity of the wave beam. It is therefore essential to consider these phenomena when predicting the performance or analyzing the signal of an inspection process, for example using a physical simulation tool. However, the complexity of a full 3D simulation of the inspection, i.e. on a macro-scale taking into account the details of the microscopic scale (micro-scale), is not accessible, or at least unreasonable.



On the other hand, the description of elastic properties on a micro-scale is at best statistical. We assume that the distribution laws of the constant elasticity coefficients and crystallographic orientation per grain are known, as well as the distribution laws of these grains (density, size, elongation, entanglement, etc.) which describe the propagation medium at the micro-scale. These distribution laws are not a priori homogeneous over the entire propagation domain of the wave beam, but we assume that they vary sufficiently smoothly to assimilate them to a constant distribution in the neighborhood of any point over a characteristic size L_d of the same order of magnitude as L_a .

Under these hypotheses, the dual-scale approach consists of extracting from this knowledge of the micro-scale some effective properties of materials on the macro-scale in order to simulate the main wave phenomena at a reasonable cost, with a standard computer workstation. This enables sensitivity studies to be carried out as a function of the main uncertain parameters of the inspection scene. These can range from variations in the shape or position of the defect to variations in the distribution laws underlying the effective properties of the medium. In addition, and by definition, the distribution law imposes a degree of randomness on the final description of the microscopic medium. This is why a statistical study is necessary at this scale to extract a reliable effective representation of the elastic properties at the macro-scale. Simulations must therefore be carried out on two distinct scales: firstly on a micro-scale in a representative elementary volume (REV) to extract effective material properties, and then on a macro-scale for the non-destructive testing study.

Various types of simulation model are available in the literature, based either on finite element methods (FEM) [1]-[6] or on phenomenological and semi-analytical approaches [7]-[11]. Here we propose two distinct FEMs. At the micro-scale, the FEM is based on a low-order approximation supported by a fine grid over the REV [5]. At the macro-scale for which the actual medium is homogeneous or smoothly heterogeneous (continuous variation), the FEM is based on a high-order approximation [6]. The inspection of a weld is taken as an illustration. On the basis of an effective material representation which assimilates the main direction of anisotropy to that of grain elongation in the chamfer, the simulation is first carried out at the macro-scale in section 2. Next, the two-scale approach is presented for the welded part, which is assimilated to ferritic and austenitic steels in section 3: FEM is deployed at the micro-scale in the REV to extract the effective properties, which are then exploited in the macro-scale simulation. The current limitations of these solutions and work in progress are discussed in section 4. In particular, structural noise on the macro-scale simulated signal is not addressed here.

2. Inspection FEM simulation at the macro-scale

A high-order approximation (in practice of order 2 to 5) significantly reduces numerical dispersion phenomena. When the main discontinuities in geometry and elastic properties remain a few characteristic lengths apart, it is possible to restrict the number of average degrees of freedom per wavelength for a given level of accuracy, almost independently of the propagation distance simulated. Under the above assumptions, the representation of a micro-structured medium as an effective homogeneous or smoothly heterogeneous medium on the macro-scale does not degrade the performance of a high-order approximation. Combining this with a condensation of the mass matrix to obtain an explicit transient model, and with a factorization of the stiffness matrix to alleviate memory constraints, such as the spectral element method (SEM) [12], gives access to a high-order approximation for 3D configurations of a few tens of wavelengths per side on standard PCs.

In recent years, CEA has developed a version of SEM dedicated to ultrasonic inspection [13] [14]. This involves taking into account fluid-structure coupling for immersion sensors and thin layers for contact sensors, viscoelasticity models to simulate attenuation, and perfectly absorbing layers to restrain the calculation domain. A domain decomposition approach facilitates the cohabitation of different propagation media in the simulated inspection scene. In addition, hybridization with the CIVA paraxial ray tracing model in the coupling for an immersed sensor or in the wedge of a contact sensor reduces simulation times. Additionally, a graphical user interface for the automatic construction of meshes for 2D or 2D5 (part, defect and sensor wedge described by an extruded 2D geometry, 3D simulation) scenes is currently being evaluated and should be available in the next commercial release of CIVA. In particular, this process combines unstructured meshes of triangles in CAD description parts with structured meshes of quadrilaterals if parametric parts (triangular-based prisms and hexahedrons in 3D, respectively).

This FEM model is illustrated in Figure 1 for a case of weld inspection with a contact sensor [6]. A ray tracing facilitates the definition of the spatial and temporal windows of the FEM scene (top image). The weld bevel and complex crack area is meshed in triangles (bottom images, brown color) while the rest of the part is meshed in regular quadrilaterals (green color), as well as the sensor wedge (beige color, dark beige in the PML domain) which interfaces with the ray-tracing simulation (red dotted line). A thin layer is visible in the lower left-hand corner between the wedge and the part. The continuously variable effective properties associated with the chamfer are illustrated in the top right-hand corner by a mapping of the principal anisotropy orientation, assimilated to the grain elongation direction, for the elastic constants summarized in Table 1. The mapping presented was obtained using the MINA phenomenological software tool [7], and preliminary work carried out at the microscopic scale corroborates the relevance of this effective representation.

Taking these effective properties into account affects the inspection prediction as illustrated in Figure 2 for a defect located in the weld bevel: without specific material properties within the bevel on the left, with a smoothly varying anisotropy orientation in the middle, and with attenuation on the right. These results confirm the importance of simulation for carrying out sensitivity studies on a macro-scale, and therefore the need for tools for predicting the effective material properties on this scale.

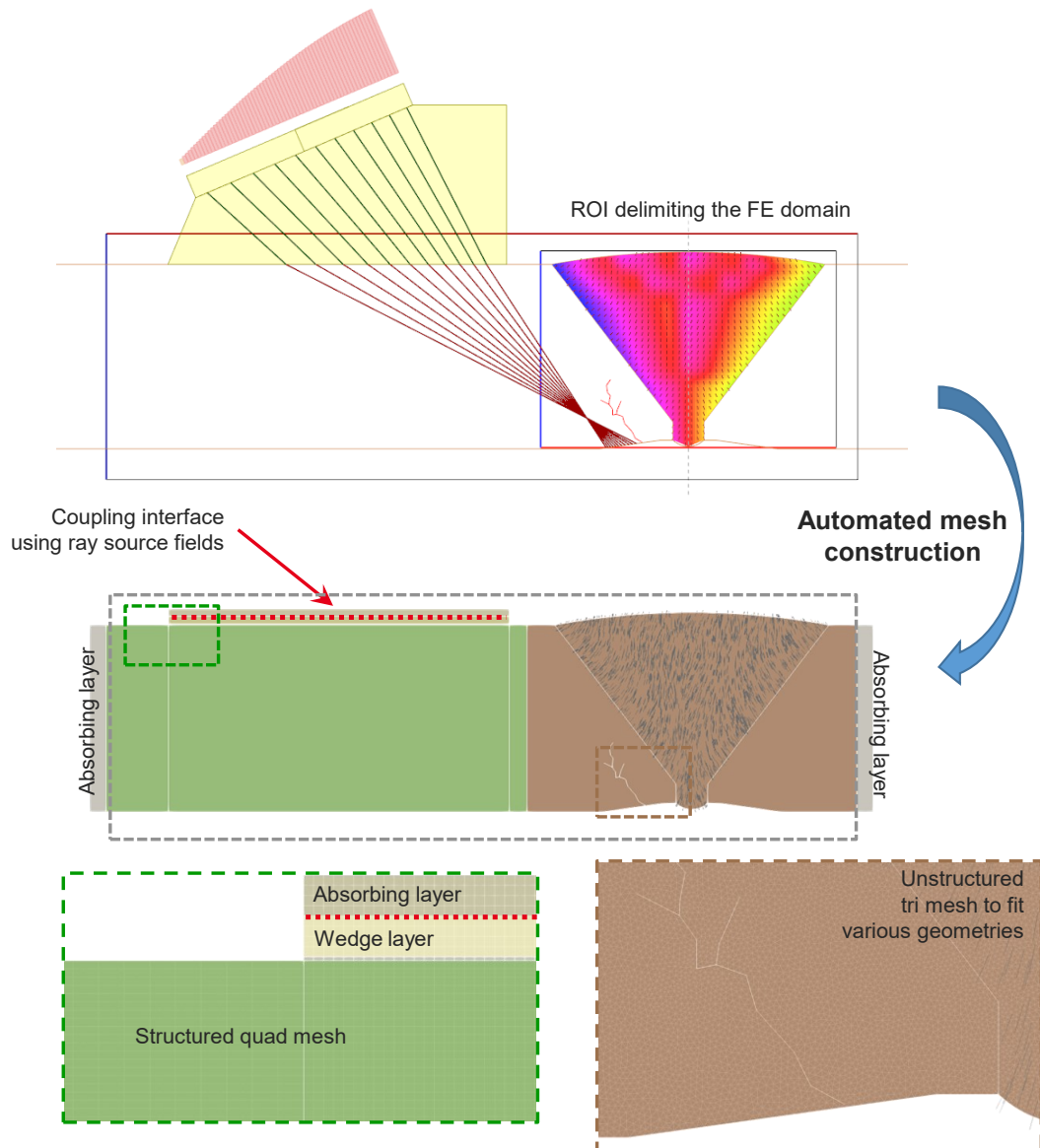


Figure 1: Example of mesh construction used to perform an FE calculation with an unstructured triangular mesh in the area around the smoothly heterogeneous bevel and structured quadrangular parts elsewhere if possible.

Table 1. Complex stiffness coefficients used for effective austenitic weld properties inspired from [15].

Effective stiffnesses (GPa)	C_{11}	$C_{22}=C_{33}$	$C_{12}=C_{13}$	C_{23}	C_{44}	$C_{55}=C_{66}$
Real part	220	245	135	110	80	110
Imaginary part	1.6	12	2	2.5	2.7	4.3

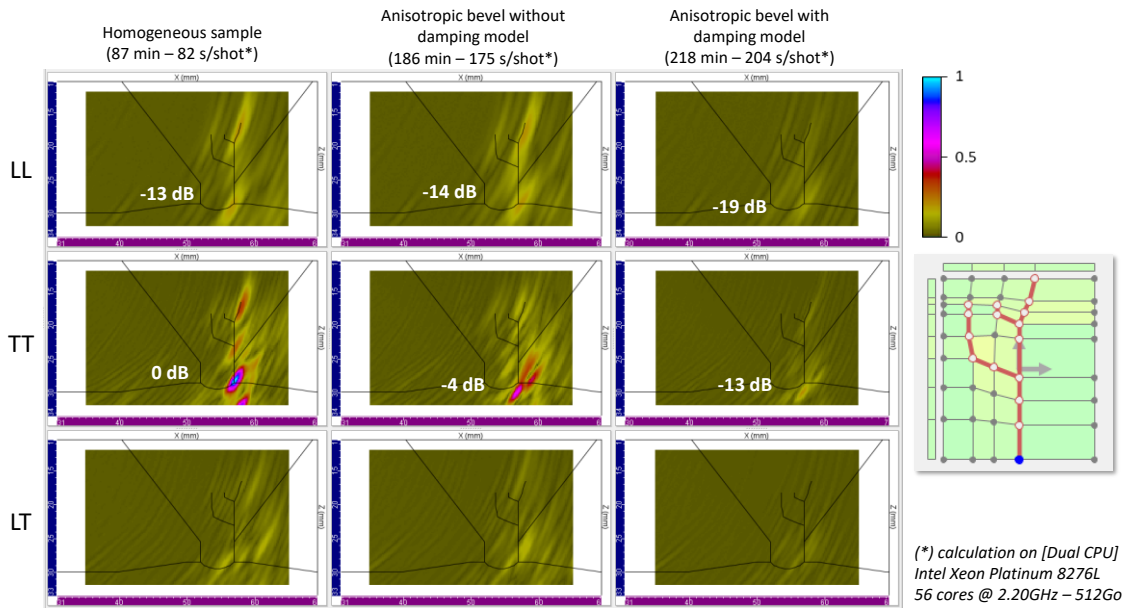


Figure 2: FE simulations of TFM imaging of a defect positioned on the left side of the bevel and comparisons considering three different descriptions for the weld material: the homogeneous isotropic case (left), the smoothly heterogeneous case without attenuation (middle) and with attenuation (right).

3. Effective material properties FEM simulation at the micro-scale

Ferritic and austenitic steels are now considered. The material properties describing these steels (i.e. at the micro-scale in each grain) are described in Table 2.

Table 2. Properties of ferrite and austenite [16].

Material	P ($\text{g}\cdot\text{cm}^{-3}$)	C11 (GPa)	C12 (GPa)	C44 (GPa)
Ferrite	7.8	231.5	135	116
Austenite	8	198	125	122

Two grain densities were considered: 512 and 64 grains per cubic millimeter. They correspond respectively to grain sizes of 125 and 250 micrometers, if the grain size is defined as the cube root of the average grain volume. Velocities and attenuations for longitudinal and shear waves were determined through finite element simulations on representative elementary volumes using a dedicated simulation tool [5]. An example of simulation used for this characterization is shown Figure 3. A microstructure is randomly generated in a rectangular volume using Voronoi tessellations, and grain orientations are randomly affected. The microstructure is made to be periodic at the lateral boundaries of the volume. A Finite Elements computation with lateral periodic boundary conditions is performed: a uniform loading is applied at the top boundary, so as to make a plane wave propagate vertically in. The resulting wave is perturbed by the microstructure. Its average over the section is computed in order to obtain an approximation of a coherent plane wave and its evolution as a function of depth. An analysis is performed in the frequency domain in order to obtain the attenuation (from the amplitude loss of the wave as a function of depth) and the phase velocity (from its phase shift). The results are attenuation and velocity for a series of frequencies in the bandwidth of the emitted wave.

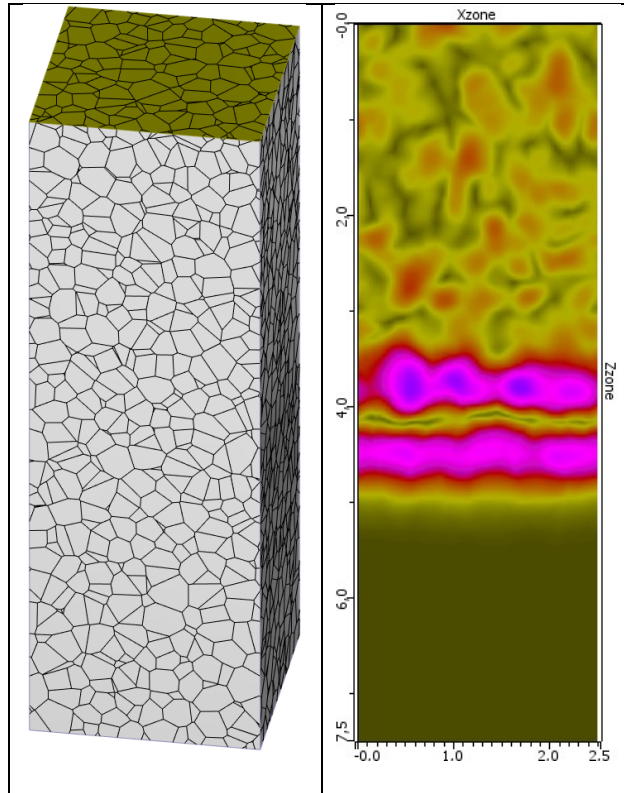
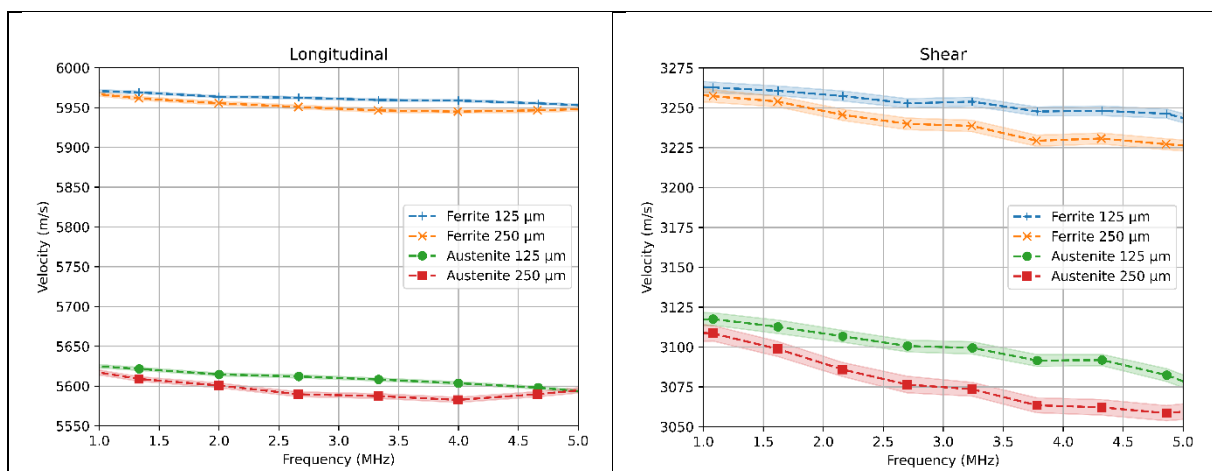


Figure 3: Simulation for a representative elementary volume of austenitic steel with 250 μm grains, representative elementary volume (left) and propagation of a longitudinal wave (right)

This procedure was applied for ferrite and austenite, for the two grain sizes, and for longitudinal and shear waves. The simulation was set so that the width of the sample contain 10 grains, and a grain correspond to 10 cells of the computation grid. 50 random realizations were computed and analyzed for each case. The procedure took approximately 5 hours of computation time on a laptop for each case. Characterization results are shown Figure 4. The curves correspond to the results averaged over the 50 realizations. The 95% confidence intervals are also indicated.



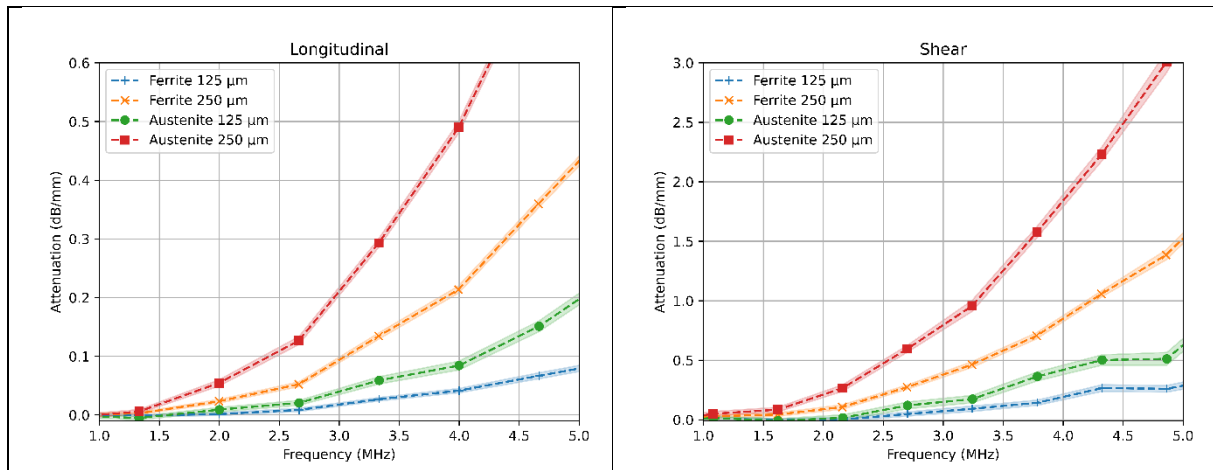


Figure 4: Velocities and attenuations as a function of frequency for the two modes and the four material/size combinations

Several expected trends are expected: shear waves are more attenuated than longitudinal wave, the larger grain size causes more attenuation, and austenite causes more attenuation than ferrite. Input parameters for the macro-scale CIVA simulations were determined using the characterization results, and are summarized in the following Table 3.

Table 3. Input parameters for CIVA simulations.

Material	vL at 2.25 MHz (m/s)	vS at 2.25 MHz (m/s)	α_L at 2.25 MHz (dB/mm)	Exponent of frequency dependency of α_L at 2.25 MHz	α_S at 2.25 MHz (dB/mm)	Exponent of frequency dependency of α_S at 2.25 MHz
Ferrite with 125 μm grains	5963	3257	0.0041	3.9	0.0090	3.9
Ferrite with 250 μm grains	5954	3245	0.034	3.7	0.13	3.5
Austenite with 125 μm grains	5614	3106	0.013	3.9	0.033	3.9
Austenite with 250 μm grains	5597	3084	0.082	3.6	0.32	3.5

As an example, these parameters are used in the simulation of a TFM inspection at 2.25 MHz of a crack at the front of the weld, as illustrated Figure 5. The results obtained in Figure 6 once again confirm the criticality of describing effective material properties in inspection simulation, on the one hand, and the criticality of macro-scale simulation for optimizing the reconstruction of TFM images, on the other.

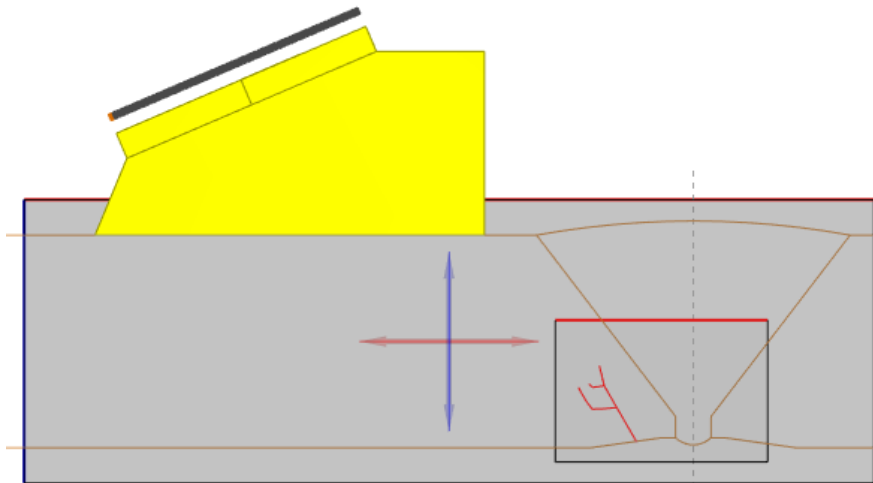


Figure 5: CIVA inspection simulation configuration

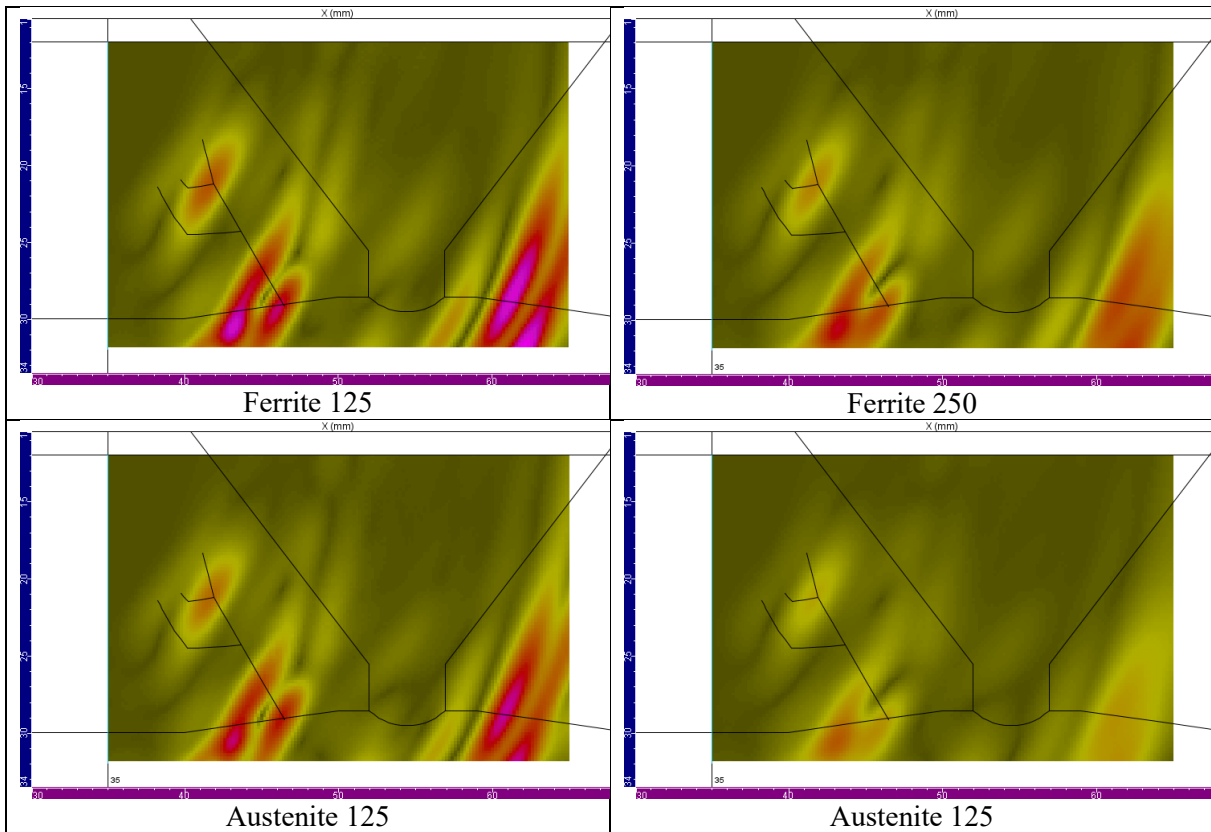


Figure 6: TFM reconstructions using the longitudinal mode for the four combination of material and grain size, with the same amplitude reference.

4. Conclusion and Perspective

Two distinct FEMs are used. The first is based on a low-order approximation grid of a representative elementary volume adapted to a highly heterogeneous distribution of material properties at the microscopic grain scale. It is used to extract an effective representation of material properties at the macroscopic inspection scale. The second FEM is based on a high-

order approximation and several optimizations to simulate the inspection on the basis of these effective material properties at the macro-scale.

These simulation tools are integrated into a development version of CIVA that is currently being evaluated, and should gradually become available. This two-scale simulation principle is illustrated section 3 for a ferritic or austenitic steel in a welded part (equi-axial grains with isotropic elastic properties at the micro-scale). Its extension to elongated and/or anisotropic grains, as in the weld bevel, is suggested in section 2, but remains limited at this stage to macro-scale simulation. Indeed, while micro-scale simulation is already possible [5], the automation of these simulation tools and, above all, of the effective properties extraction in such media, is still in progress. In the longer term, we aim to create a database of REV's simulated over a range of variations in the micro-scale description (grain shape and density, etc.) to feed into a smoothly heterogeneous macro-scale effective medium.

References

- [1] B. Chassignole, V. Duwig, M. A. Ploix, P. Guy, R. El Guerjouma, 'Modelling the attenuation in the athena finite elements code for the ultrasonic testing of austenitic stainless steel welds', *Ultrasonics* 49 (8) (2009) 653–658. <https://doi:10.1016/j.ultras.2009.04.001>
- [2] M. Dunlap, G. Connolly, J. Dobson, 'Modeling and Simulation of Cast Austenitic Stainless Steel with OnScale', in: 2020 IEEE International Ultrasonics Symposium (IUS), 2020, pp. 1–4, iSSN: 1948-5727. <https://doi:10.1109/IUS46767.2020.9251616>
- [3] [POGO1] M. Huang, G. Sha, P. Huthwaite, S. I. Rokhlin, M. J. S. Lowe, 'Maximizing the accuracy of finite element simulation of elastic wave propagation in polycrystals', *The Journal of the Acoustical Society of America* 148 (4) (2020) 1890–1910. <https://doi:10.1121/10.0002102>
- [4] M. Huang, P. Huthwaite, S. I. Rokhlin, M. J. S. Lowe, 'Finite-element and semi-analytical study of elastic wave propagation in strongly scattering polycrystals', *Proceedings of the Royal Society A: Mathematical, Physical and Engineering Sciences* 478 (2258) (2022) 20210850. <https://doi:10.1098/rspa.2021.0850>
- [5] V. Dorval, N. Leymarie, A. Imperiale, E. Demaldent, Z. Aghenzour and P.-E. Lhuillier, 'Determining ultrasonic propagation effective properties in complex heterogeneous media through microstructure-scale simulation', *Papers of the ECNDT 2023, ReJNDT*, vol. 1(1), Aug. 2023, <https://doi:10.58286/28132>
- [6] N. Leymarie, A. Imperiale, J. Barras, P. Lhuillier, A. Schumm, Y. Gélébart and E. Demaldent, 'TFM imaging simulations of defects near or in the weld bevel: modelling approach and customized finite element tools', *NDE in Nuclear 2023*, June, Hall in Sheffield, United Kingdom, *e-Journal of Nondestructive Testing* Vol. 28(10). <https://doi.org/10.58286/28707>
- [7] J. Moysan, G. Corneloup, B. Chassignole, C. Gueudré, and M. A. Ploix, "Modelling welded material for ultrasonic testing using MINA: Theory and applications," *AIP Conference Proceedings*, vol. 1430, no. 1, pp. 1219–1226, May 2012, <https://doi:10.1063/1.4716358>
- [8] J. A. Ogilvy, 'Computerized ultrasonic ray tracing in austenitic steel', *NDT International* 18 (2) (1985) 67–77. [https://doi:10.1016/0308-9126\(85\)90100-2](https://doi:10.1016/0308-9126(85)90100-2)
- [9] N. Gengembre, A. Lhémy, 'Calculation of wideband ultrasonic fields radiated by water-coupled transducers into heterogeneous and anisotropic media', *AIP Conference Proceedings* 509 (1) (2000) 977–984. <https://doi:10.1063/1.1306150>

- [10]V. Dorval, F. Jenson, G. Corneloup, J. Moysan, ‘Accounting for structural noise and attenuation in the modeling of the ultrasonic testing of polycrystalline materials’, AIP Conference Proceedings 1211 (1) (2010) 1309–1316. <https://doi:10.1063/1.3362219>
- [11]R. E. Jacob, M. S. Prowant, M. S. Hughes, A. A. Diaz, ‘Modeling and Simulation of Austenitic Welds and Coarse-grained Specimens: Part II’, Tech. Rep. PNNL-32702, Pacific Northwest National Laboratory (PNNL), Richland, WA (United States) (Mar. 2022). <https://doi:10.2172/1988074>
- [12]D. Komatitsch and J. Tromp, ‘Introduction to the spectral element method for three-dimensional seismic wave propagation,’ Geophys J Int, vol. 139, no. 3, pp. 806–822, Dec. 1999, <https://doi:10.1046/j.1365-246x.1999.00967.x>
- [13]A. Imperiale and E. Demaldent, ‘A macro-element strategy based upon spectral finite elements and mortar elements for transient wave propagation modeling. Application to ultrasonic testing of laminate composite materials’, International Journal for Numerical Methods in Engineering, vol. 119, no. 10, pp. 964–990, 2019, <https://doi:10.1002/nme.6080>
- [14]A. Imperiale, N. Leymarie, and E. Demaldent, ‘Numerical modeling of wave propagation in anisotropic viscoelastic laminated materials in transient regime: Application to modeling ultrasonic testing of composite structures’, International Journal for Numerical Methods in Engineering, vol. 121, no. 15, pp. 3300–3338, 2020, <https://doi:10.1002/nme.6359>
- [15]P. Guy, B. Mascaro, M. Darmon, N. Leymarie, and B. Clausse, ‘Accurate experimental determination of the complex elastic tensor of anisotropic materials of unknown orientation using ultrasonic transmitted bulk waves’, in 2019 International Congress on Ultrasonics, Bruges, Belgium, Sep. 2019. Accessed: May 25, 2021. [Online]. Available: <https://hal.archives-ouvertes.fr/hal-02316999>
- [16]A. Duijster, A. Volker, F. Van den Berg and C. Celada-Casero, ‘Estimation of Grain Size and Composition in Steel Using Laser UltraSonic Simulations at Different Temperatures’, Applied Sciences, vol. 13, no. 2, p. 1121, Jan. 2023, <https://doi:10.3390/app13021121>